Published in final edited form as:
J Magn Reson Imaging. 2013 October ; 38(4): 868–875. doi:10.1002/jmri.24042.

The Effects of Perfusion on Diffusion Changes in Human Brain Tumors

Alexander D. Cohen, BS[1,3], **Peter S. LaViolette, PhD**[2], **Melissa Prah, BS**[2], **Jennifer Connelly, MD**[3,4], **Mark G. Malkin, MD**[3,4,5], **Scott D. Rand, MD, PhD**[2,3], **Wade M. Mueller, MD**[3,5], and **Kathleen M. Schmainda, PhD**[1,2,3]

[1]Department of Biophysics, Medical College of Wisconsin, 8701 Watertown Plank Rd. Milwaukee, WI 53226

[2]Department of Radiology, Medical College of Wisconsin, 8701 Watertown Plank Rd. Milwaukee, WI 53226

[3]Department of Translational Brain Tumor Research Program, Medical College of Wisconsin, 8701 Watertown Plank Rd. Milwaukee, WI 53226

[4]Department of Neurology, Medical College of Wisconsin, 8701 Watertown Plank Rd. Milwaukee, WI 53226

[5]Department of Neurosurgery, Medical College of Wisconsin, 8701 Watertown Plank Rd. Milwaukee, WI 53226

Abstract

Purpose—To characterize the influence of perfusion on the measurement of diffusion changes over time when ADC is computed using standard two-point methods.

Materials and Methods—Functional diffusion maps (FDMs), which depict changes in diffusion over time, were compared to rCBV changes in patients with brain tumors. The FDMs were created by coregistering and subtracting ADC maps from two time points and categorizing voxels where ADC significantly increased (iADC), decreased (dADC), or did not change (ncADC). Traditional FDMs (tFDMs) were computed using b=0,1000 s/mm^2. Flow-compensated FDMs (fcFDMs) were calculated using b=500,1000 s/mm^2. Perfusion's influence on FDMs was determined by evaluating changes in rCBV in areas where the ADC change significantly differed between the two FDMs.

Results—The mean ΔrCBV in voxels that changed from iADC (dADC) on the tFDM to ncADC on the fcFDM was significantly greater (less) than zero. In addition, mean ΔrCBV in iADC (dADC) voxels on the tFDM was significantly higher (lower) than in iADC (dADC) voxels on the fcFDM.

Conclusion—The ability to accurately identify changes in diffusion on traditional FDMs is confounded in areas where perfusion and diffusion changes are co-localized. Flow-compensated FDMs, which use only non-zero b-values, should therefore be the standard approach.

Keywords

Functional diffusion map; diffusion; perfusion; ADC; brain tumor; b-value

Corresponding Author: Kathleen M. Schmainda, PhD, Medical College of Wisconsin, Department of Biophysics, 8701 Watertown Plank Road, Milwaukee, WI 53226, Phone: 414-955-4051, Fax: 414-955-6512, kathleen@mcw.edu.

INTRODUCTION

Malignant primary brain tumors account for two percent of all adult cancers in the United States, with neuroglial tumors representing 80% and meningeal tumors representing 20% of all central nervous system tumors (1). The World Health Organization classifies glial brain tumors into four grades. Grades 1 and 2 are categorized as low grade and grades 3 and 4 as high grade (2). Treatment for brain tumors includes surgery (3, 4), and either radiation, chemotherapy, or a combination of the two (5–8). The response of a tumor to treatment is typically assessed using pre and post contrast anatomical T1 weighted images (9). This method assesses tumor response by measuring the change in the enhancing tumor area over time. Despite its widespread use, it has become clear that this approach may be too simplistic and is insufficient for accurately monitoring tumor response (10).

As a result, more advanced imaging techniques have been developed and used to assess tumor response, including FLAIR, which highlights edema, diffusion weighted MRI (DWI), which is sensitive to tumor microstructure, and dynamic susceptibility contrast MRI (DSC), which measures blood perfusion. A DWI-based technique for measuring treatment response and tumor progression called functional diffusion maps (FDMs) has recently been described (11–15). FDMs are created by subtracting apparent diffusion coefficient (ADC) images from two imaging sessions, separated by days or weeks, resulting in an ADC difference map. The voxels are then classified as either having increased (iADC), or decreased ADC (dADC), or having no change in ADC (ncADC) based on previously determined thresholds (11). FDM-derived metrics have been shown to correlate with overall survival in high grade glioma (12), predict survival in glioblastoma multiforme (GBM) before and after radiochemotherapy (13), and have been shown to be a predictive imaging biomarker following cytotoxic and anti-angiogenic treatments (14). Graded FDMs, which display voxels at several additional levels of ADC changes also predict survival in GBMs treated with bevacizumab (15).

ADC has been shown to be inversely proportional to cell density (16–19). As such, FDMs have been used to estimate changes in tumor cellularity over time. The terms “hypocellular” and “hypercellular” have been used to describe voxels in which ADC has increased and decreased respectively. These terms, however, can be misleading, as cell density is not the only factor that influences ADC. Other reasons include infection (20, 21), edema (22, 23), and subacute stroke (24). Another possible confound to FDMs is perfusion, as diffusion MRI can be made sensitive to blood flow, an approach previously referred to as the intravoxel incoherent motion (IVIM) method (25–28). As tumors grow, they stimulate the growth of new blood vessels through a process called pathologic angiogenesis (29). As new vessels are created or recede as a result of successful treatment, ADC in that area increases or decreases respectively. This is due to ADC typically being calculated with b = 0 s/mm^{2}which contains blood flow contributions. ADC calculated with higher b-values (> 200 s/mm^2) in place of b = 0 s/mm^2 is not confounded by contributions from moving blood, as the signal from the fast moving blood is sufficiently suppressed (28, 30, 31). Despite this previous work most clinical DWI studies still calculate ADC maps using b-values of 0 and 1000 s/mm^{2}and accordingly much of the literature demonstrating the utility of FDMs is based on DWI data obtained at these b-values. In this context the influence of perfusion on FDMs, obtained from traditional DWI data, has not been characterized.

In this study we characterized the influence of perfusion effects on FDM calculations. This was addressed by generating two sets of FDMs, which were then compared. The first used b = 0 and 1,000 s/mm^2 in the calculation of ADC to create traditional FDMs, (tFDMs). The second used a higher b-value (b = 500 s/mm^2) in place of b = 0 s/mm^2 in the calculation of ADC to create flow compensated FDMs (fcFDMs). To assess the actual blood perfusion

contribution, the change in relative cerebral blood volume (rCBV) was calculated from DSC images and then assessed in voxels that differed in classification between the two FDMs (i.e. iADC voxel on FDM, ncADC voxel on fcFDM).

We hypothesized that voxels classified as iADC or dADC on the tFDM solely due to perfusion changes would subsequently be classified as ncADC on the fcFDM, as the fcFDM is calculated using perfusion insensitive ADC values. Furthermore, we hypothesized that the "classification-changing" voxels would show a significant change in rCBV (ΔrCBV). In other words, voxels classified as iADC on the tFDM and ncADC on the fcFDM would have a positive ΔrCBV as an increase in perfusion from the first time-point (TP1) to the second time-point (TP2) mimicked a decrease in cellularity. On the other hand, voxels classified as dADC on the tFDM and ncADC on the fcFDM would have a negative ΔrCBV as a decrease in perfusion from TP1 to TP2 mimicked an increase in cellularity.

MATERIALS AND METHODS

Subjects

Data from thirty patients (21 male, 9 female) from our brain tumor imaging database was retrospectively analyzed. This data set included 8 WHO Grade 4 GBM, 12 WHO Grade 3 lesions (6 anaplastic astrocytomas, 3 oligodendrogliomas, and 3 mixed astrocytoma/oligodendrogliomas), and 10 low-grade gliomas (2 astrocytomas, 3 oligodendrogliomas, 4 mixed astrocytoma/oligodendrogliomas, and 1 suspected meningioma). Written informed consent, approved by our institutional review board (IRB), was obtained from each patient. Inclusion criteria for this study included at least two scans on a Siemens Espree 1.5T (Espree) scanner during which FLAIR, DWI (with b=0, 500, and 1000s/mm^2), and DSC perfusion imaging data were acquired.

Imaging

All data was analyzed retrospectively. T1-weighted SPGR anatomical images were acquired using the following parameters: TE/TR = 4.76/11.0 ms, flip angle (FA) = 15°, FOV = 19.2 cm, matrix = 192×256, voxel size = 1.0×1.0×1.3 mm and 112 or 128 slices. T2-weighted FLAIR images were acquired with the following parameters: TE/TR = 90/10,000 ms, FA = 150°, FOV = 19.2 cm, matrix = 280×320, voxel size = 0.69×0.69×6.5 mm and 22 or 24 slices. DWI images were collected using a spin-echo (SE) EPI sequence using diffusion weightings (b-values) of b = 0, 500, and 1,000 s/mm^2. DWI was collected with the following parameters: TE/TR = 98/3,900 ms, FA = 90°, FOV = 23.0 cm, matrix = 128×128, voxel size = 1.80×1.80×6.5 mm and 22 or 24 slices. Just before imaging for DSC, a 0.05 to 0.1 mmol/kg (pre-load) dose of Gadolinium (Gd) contrast agent was administered. The pre-load dose reduces unwanted T1-weighted effects resulting from contrast agent leaking into the extravascular space that confound the rCBV measurements derived from the dynamic susceptibility contrast (DSC) data (32–34). Single shot gradient-echo (GE) EPI was used to collect images during a second 0.1 mmol/kg bolus of Gd injected at a rate of 3–5 mL/s. DSC data was acquired with the following parameters: TE/TR = 30/1,100 ms, flip angle (FA) = 72°, FOV = 22.0 cm, matrix = 96×96, voxel size = 2.29×2.29×6.5 mm, and 13 slices.

Functional Diffusion Maps (FDMs)

Two sets of FDMs were calculated. The tFDM was processed using ADC calculated from b-values of 0 and 1,000 s/mm^2. The fcFDM was processed using ADC calculated from b-values of 500 and 1,000 s/mm^{2}where for both voxelwise ADC calculations:

$$\mathrm{ADC}=\frac{1}{1000-b_n}\cdot\ln\left(\frac{S_n}{S_{1000}}\right) \quad [1]$$

where b_n was either 0 or 500 s/mm^2, S_n was the signal of the b_0 or b_{500} image, and S_{1000} was the signal from the b_{1000} image. Apart from the differing b-values, the processing steps for the tFDMs and fcFDMs were identical. The tFDMs and fcFDMs were calculated for each patient from two time-points (TP1 and TP2). First, ADC was calculated for both TP1 and TP2 on a voxelwise basis from the DWI data using Equation 1 in AFNI (35). All images from each patient were registered to their own SPGR from TP1 with a rigid-body, mutual information algorithm with 6 degrees of freedom using FLIRT (36) (FSL, FMRIB tool library). All images from TP1 were directly registered to the SPGR from TP1. Images from TP2 were first registered to the SPGR from TP2. The SPGR from TP2 was then registered to the SPGR from TP1, and the registration matrix was output. This matrix was then used to register the remaining TP2 images to the SPGR from TP1. The result was all images coregistered to the SPGR from TP1. A visual inspection was performed to ensure accurate registration. Next, the ADC images from the two time-points were subtracted on a voxelwise basis to create ΔADC maps and masked by the FLAIR abnormality from TP1 and TP2 inclusive. These maps were then thresholded based on a previously determined cutoff value of 4.0×10^{-4} s/mm^2 (16). Voxels where ADC increased (iADC) above this threshold were colored red. Voxels where ADC decreased (dADC) below this threshold were colored blue, and voxels with no significant change in ADC (ncADC) were colored green. While this threshold was derived from measurements in gray matter and normal appearing white matter, it was found to have the greatest sensitivity and specificity compared to various other threshold values when applied to FLAIR abnormal regions on FDMs (16).

DSC Post-processing

Voxelwise images of rCBV were calculated from the DSC data using methods previously published (32–34, 37) with a leakage corrected trapezoidal integration followed by intensity standardization (38, 39) as implemented in the IBNeuro software package v1.1 (www.imagingbiometrics.com). The rCBV images from TP1 and TP2 were co-registered to the SPGR from TP1 using the methods described above.

Perfusion Effects on Diffusion

To evaluate the effects of perfusion on the resulting ΔADC maps the tFDMs and fcFDMs were compared with the rCBV maps. As mentioned, the tFDMs were created with ADC maps produced with b=0 and 1000 s/mm^{2}while the fcFDMs were created with ADC maps produced with b=500 and 1000 s/mm^2. Figure 1 shows the difference between flow sensitive, and flow compensated ADC maps. Schematic differences between tFDMs and fcFDMs are shown in Figure 2.

Data Analysis

To determine the perfusion effects on tFDMs, mean ΔrCBV was calculated in areas that changed from increasing ADC ($iADC_{tFDM}$) and decreasing ADC ($dADC_{tFDM}$) on the tFDM to no change in ADC on the fcFDM ($ncADC_{fcFDM}$) (i.e. red or blue voxels on tFDM to green voxels on fcFDM). Mean ΔrCBV was also calculated in $iADC_{tFDM}$ and $dADC_{tFDM}$ voxels that did not change categories on fcFDMs. These values were tested against the null-hypothesis, that there was no change in rCBV, using a one-sample t-test. They were additionally compared to one another using an unpaired two-sample t-test. In addition, mean ΔrCBV was calculated separately for all $iADC_{tFDM}$ and $dADC_{tFDM}$ voxels and compared to the mean ΔrCBV calculated separately for all $iADC_{fcFDM}$ and $dADC_{fcFDM}$ voxels. The results were compared using an unpaired two-sample t-test. Finally, the percentage of

$iADC_{tFDM}$, $dADC_{tFDM}$ and $ncADC_{tFDM}$ that changed categories on the fcFDM was calculated and compared. All statistical analyses were performed in Matlab (Mathworks, Natick, MA). Results were considered significant if $p < 0.05$.

RESULTS

Figure 3 shows scatter plots of ADC from TP2 versus ADC from TP1 from two representative patients. The *color* of the dots is dictated by the direction of change of the rCBV with red colors indicating positive ΔrCBV and blue colors indicating negative ΔrCBV. The *location* of the dots on the plots is dictated by the direction of change in ADC. Specifically, dots in the upper left region of the plot, above the upper diagonal line, were classified as iADC, while dots in the lower right region of the plot, below the lower diagonal line, were classified as dADC. The plots in column 1 show all voxels classified as either iADC or dADC on the tFDM and the column 2 plots show those *same* voxels on the fcFDM. In general, iADC voxels tended to have positive ΔrCBV, and dADC voxels tended to have negative ΔrCBV. The $iADC_{tFDM} \rightarrow ncADC_{fcFDM}$ voxels had a positive ΔrCBV, and $dADC_{tFDM} \rightarrow ncADC_{fcFDM}$ voxels had a negative ΔrCBV. The plots shown in columns 3 and 4 show voxels characterized as $ncADC_{tFDM}$. These voxels tended to have low ΔrCBV and to not change categories on the fcFDM.

These results are quantified in Figure 4 and Table 1. The bar chart in Figure 4A shows the percentage of voxels classified as $dADC_{tFDM}$, $ncADC_{tFDM}$, and $iADC_{tFDM}$ that changed categories following flow compensation on the fcFDM. The percentage of $dADC_{tFDM}$ and $iADC_{tFDM}$ voxels that changed categories (52.9% and 52.6% respectively) was significantly higher than the percentage of $ncADC_{tFDM}$ voxels that changed categories (4.7%, $p<0.001$).

The mean ΔrCBV in these category-changing voxels is displayed in Figure 4B. Mean ΔrCBV in $iADC_{tFDM} \rightarrow ncADC_{fcFDM}$ voxels was significantly greater than zero, (1.26 (0.37) a.u., one-sample t-test, p=0.002) and significantly differed from ΔrCBV in voxels that did not change from the tFDM to the fcFDM (unpaired two sample t-test, $p = 0.03$), as well as $dADC_{tFDM} \rightarrow ncADC_{fcFDM}$ voxels (unpaired two sample t-test, $p < 0.001$). Mean ΔrCBV in $dADC_{tFDM} \rightarrow ncADC_{fcFDM}$ voxels was significantly less than zero (−0.97 (0.35) a.u., one-sample t-test, p=0.01) and significantly differed from ΔrCBV in voxels that did not change from tFDM to fcFDM (unpaired two sample t-test, $p = 0.001$). Mean ΔrCBV in tFDM voxels that did not change categories on the fcFDM was not significantly different from zero, (−0.086 (0.25) a.u., one-sample t-test, $p = 0.73$).

Mean ΔrCBV in all tFDM and fcFDM voxels is shown in Figure 4C. Mean ΔrCBV in $iADC_{tFDM}$ voxels was significantly higher than in $iADC_{fcFDM}$ voxels ($p<0.001$). Mean ΔrCBV in $dADC_{tFDM}$ voxels was significantly lower than in $dADC_{fcFDM}$ voxels (p=0.01), and there was no difference in mean ΔrCBV in $ncADC_{tFDM}$ compared to $ncADC_{fcFDM}$ voxels (p=0.21). Representative examples of category changing voxels are shown Figure 5. The tFDMs are shown along side fcFDMs and their corresponding ΔrCBV maps.

DISCUSSION

This study examined rCBV changes over time in areas where there were diffusion changes over time (ie FDMs) and showed the confounding effect that perfusion changes can have on functional diffusion maps. These effects can be diminished by calculating ADC from DWI data that does not include b-values less than 200 s/mm^2. Though this perfusion correction appears to compensate for falsely classified FDM voxels, a ground truth histological validation is necessary to be certain. As demonstrated in this study, we found that voxels categorically changing from increased ADC on the traditional FDM to no change in ADC on

the flow-compensated FDM had an increase in perfusion from timepoint 1 to timepoint 2, and voxels categorically changing from decreased ADC on the traditional FDM to no change in ADC on the flow compensated FDM had a decrease in perfusion from timepoint 1 to timepoint 2,. These results are consistent with our hypothesis that tFDMs are susceptible to changes in ADC due solely to perfusion changes.

These conclusions suggest that perfusion effects on FDMs can be avoided by using only diffusion data collected at b-values greater than 200 s/mm^2 to calculate ADC. This idea has been presented before. A recent paper summarizing the National Cancer Institute (NCI) Diffusion MRI Consensus Conference put forth recommendations for using DWI to monitor cancer treatment response (40). They recommended collecting a minimum of three b-values, including b = 0, b > 100, and b > 500 s/mm^{2}and using the two higher b-values to calculate perfusion-insensitive ADC values.

Numerous studies have used tFDMs to predict treatment response and/or survival in brain tumors. These studies have all used b = 0 s/mm^2 in their ADC calculations (12, 14–16) since that has been the standard way to collect DWI data in patients. The purpose of this study was to investigate how changes in perfusion affect changes in diffusion depicted with FDMs. We did not, however, evaluate how well fcFDMs predict clinical parameters. Therefore, future studies need to be undertaken to look at the ability fcFDMs to predict treatment response and survival compared to tFDMs. Theoretically, the use of fcFDMs in place of tFDMs should only enhance the ability of serial changes in ADC to predict clinical parameters and should strengthen the conclusions found by these earlier studies. A larger effect may be seen when interpreting fcFDMs on an individual basis in the clinic. Increased (decreased) perfusion from TP1 to TP2, which is assumed to be a negative (positive) prognostic indicator, may be classified as iADC (dADC) on tFDMs and be interpreted as a decrease (increase) in cellularity, which in turn is assumed to be a positive (negative) prognostic indicator (16). Removal of these opposing effects will make decisions made by the clinicians more accurate.

One of the limitations of this retrospective study was that more b-values were not collected. Previous studies have shown b-values greater than 200 s/mm^2 are sufficient to suppress the signal from blood flow (26, 31, 40). Therefore, while the b-value used here (b = 500 s/mm^2) was sufficient to suppress blood flow it may not be the optimal choice. SNR decreases with increasing b-value and, as a result, ADC calculated using higher b-values is more susceptible to variations in noise. Therefore, smaller non-zero b-values, closer to b = 200 s/mm^{2}may provide better ADC estimates.

Finally, this study used functional diffusion maps to look at changes in blood flow defined in areas where ADC significantly changed. Another way to perform this analysis would have been to look at changes in diffusion defined by areas where perfusion significantly changed. The former analysis method was chosen because tFDMs have been validated as a treatment response biomarker, and a value that says what constitutes a “significant” change in ADC has been rigorously defined (16). This is not the case for rCBV measures. Furthermore, since tFDMs use changes in ADC to predict treatment response and survival, it is important to know the effects of perfusion on the tFDMs themselves. The rCBV measure is sensitive to tumor grade and predictive of survival (26, 31, 40), however, serial changes in rCBV have not been thoroughly assessed in terms of their predictive ability.

In conclusion, this study used a higher b-value (b = 500 s/mm^2) in place of b = 0 s/mm^2 to calculate ADC, resulting in flow compensated FDMs. The results suggest that these maps are less sensitive to perfusion effects. We therefore recommend using higher b-values (>200

s/mm^2) when examining changes in ADC over time as perfusion changes can be falsely classified as cellularity changes.

Acknowledgments

The authors would like to thank Cathy Marszalkowski for administrative support, and the patients for participating in the imaging studies.

Grant Support: Funding support was provided by NIH/NCI 2 RO1 CA082500, Advancing a Healthier Wisconsin and the MCW Translational Brain Tumor Research Program.

REFERENCES

1. Chandana SR, Movva S, Arora M, Singh T. Primary brain tumors in adults. Am Fam Physician. 2008; 77(10):1423–1430. [PubMed: 18533376]
2. Louis DN, Ohgaki H, Wiestler OD, et al. The 2007 WHO classification of tumours of the central nervous system. Acta Neuropathol. 2007; 114(2):97–109. [PubMed: 17618441]
3. Hentschel SJ, Sawaya R. Optimizing outcomes with maximal surgical resection of malignant gliomas. Cancer Control. 2003; 10(2):109–114. [PubMed: 12712005]
4. Hess KR. Extent of resection as a prognostic variable in the treatment of gliomas. J Neurooncol. 1999; 42(3):227–231. [PubMed: 10433106]
5. Friedman HS, Prados MD, Wen PY, et al. Bevacizumab alone and in combination with irinotecan in recurrent glioblastoma. J Clin Oncol. 2009; 27(28):4733–4740. [PubMed: 19720927]
6. Hoang-Xuan K, Capelle L, Kujas M, et al. Temozolomide as initial treatment for adults with low-grade oligodendrogliomas or oligoastrocytomas and correlation with chromosome 1p deletions. J Clin Oncol. 2004; 22(15):3133–3138. [PubMed: 15284265]
7. Stupp R, Mason WP, van den Bent MJ, et al. Radiotherapy plus concomitant and adjuvant temozolomide for glioblastoma. N Engl J Med. 2005; 352(10):987–996. [PubMed: 15758009]
8. Yu JB, Schulder M, Knisely J. Radiosurgical dose selection for brain metastasis. Prog Neurol Surg. 2012; 25:139–147. [PubMed: 22236675]
9. Macdonald DR, Cascino TL, Schold SC Jr, Cairncross JG. Response criteria for phase II studies of supratentorial malignant glioma. J Clin Oncol. 1990; 8(7):1277–1280. [PubMed: 2358840]
10. Wen PY, Macdonald DR, Reardon DA, et al. Updated response assessment criteria for high-grade gliomas: response assessment in neuro-oncology working group. J Clin Oncol. 2010; 28(11): 1963–1972. [PubMed: 20231676]
11. Hamstra DA, Chenevert TL, Moffat BA, et al. Evaluation of the functional diffusion map as an early biomarker of time-to-progression and overall survival in high-grade glioma. Proc Natl Acad Sci U S A. 2005; 102(46):16759–16764. [PubMed: 16267128]
12. Hamstra DA, Galban CJ, Meyer CR, et al. Functional diffusion map as an early imaging biomarker for high-grade glioma: correlation with conventional radiologic response and overall survival. J Clin Oncol. 2008; 26(20):3387–3394. [PubMed: 18541899]
13. Ellingson BM, Cloughesy TF, Zaw T, et al. Functional diffusion maps (fDMs) evaluated before and after radiochemotherapy predict progression-free and overall survival in newly diagnosed glioblastoma. Neuro Oncol. 2012; 14(3):333–343. [PubMed: 22270220]
14. Ellingson BM, Malkin MG, Rand SD, et al. Volumetric analysis of functional diffusion maps is a predictive imaging biomarker for cytotoxic and anti-angiogenic treatments in malignant gliomas. J Neurooncol. 2010; 102(1):95–103. [PubMed: 20798977]
15. Ellingson BM, Cloughesy TF, Lai A, et al. Graded functional diffusion map-defined characteristics of apparent diffusion coefficients predict overall survival in recurrent glioblastoma treated with bevacizumab. Neuro Oncol. 2011; 13(10):1151–1161. [PubMed: 21856685]
16. Ellingson BM, Malkin MG, Rand SD, et al. Validation of functional diffusion maps (fDMs) as a biomarker for human glioma cellularity. J Magn Reson Imaging. 2010; 31(3):538–548. [PubMed: 20187195]

17. Hayashida Y, Hirai T, Morishita S, et al. Diffusion-weighted imaging of metastatic brain tumors: comparison with histologic type and tumor cellularity. AJNR Am J Neuroradiol. 2006; 27(7): 1419–1425. [PubMed: 16908550]
18. Manenti G, Di Roma M, Mancino S, et al. Malignant renal neoplasms: correlation between ADC values and cellularity in diffusion weighted magnetic resonance imaging at 3 T. Radiol Med. 2008; 113(2):199–213. [PubMed: 18386122]
19. Sugahara T, Korogi Y, Kochi M, et al. Usefulness of diffusion-weighted MRI with echo-planar technique in the evaluation of cellularity in gliomas. J Magn Reson Imaging. 1999; 9(1):53–60. [PubMed: 10030650]
20. Gaviani P, Schwartz RB, Hedley-Whyte ET, et al. Diffusion-weighted imaging of fungal cerebral infection. AJNR Am J Neuroradiol. 2005; 26(5):1115–1121. [PubMed: 15891169]
21. Gasparetto EL, Cabral RF, da Cruz LC Jr, Domingues RC. Diffusion imaging in brain infections. Neuroimaging Clin N Am. 2011; 21(1):89–113. [PubMed: 21477753]
22. Ito J, Marmarou A, Barzo P, Fatouros P, Corwin F. Characterization of edema by diffusion-weighted imaging in experimental traumatic brain injury. J Neurosurg. 1996; 84(1):97–103. [PubMed: 8613843]
23. Eis M, Els T, Hoehn-Berlage M, Hossmann KA. Quantitative diffusion MR imaging of cerebral tumor and edema. Acta Neurochir Suppl (Wien). 1994; 60:344–346. [PubMed: 7976585]
24. van Everdingen KJ, van der Grond J, Kappelle LJ, Ramos LM, Mali WP. Diffusion-weighted magnetic resonance imaging in acute stroke. Stroke. 1998; 29(9):1783–1790. [PubMed: 9731595]
25. Henkelman RM, Neil JJ, Xiang QS. A quantitative interpretation of IVIM measurements of vascular perfusion in the rat brain. Magn Reson Med. 1994; 32(4):464–469. [PubMed: 7997111]
26. Le Bihan D, Breton E, Lallemand D, Aubin ML, Vignaud J, Laval-Jeantet M. Separation of diffusion and perfusion in intravoxel incoherent motion MR imaging. Radiology. 1988; 168(2): 497–505. [PubMed: 3393671]
27. Le Bihan D, Breton E, Lallemand D, Grenier P, Cabanis E, Laval-Jeantet M. MR imaging of intravoxel incoherent motions: application to diffusion and perfusion in neurologic disorders. Radiology. 1986; 161(2):401–407. [PubMed: 3763909]
28. Luciani A, Vignaud A, Cavet M, et al. Liver cirrhosis: intravoxel incoherent motion MR imaging--pilot study. Radiology. 2008; 249(3):891–899. [PubMed: 19011186]
29. Folkman J. Angiogenesis in cancer, vascular, rheumatoid and other disease. Nat Med. 1995; 1(1): 27–31. [PubMed: 7584949]
30. Le Bihan D, Turner R. Intravoxel incoherent motion imaging using spin echoes. Magn Reson Med. 1991; 19(2):221–227. [PubMed: 1881307]
31. Lemke A, Stieltjes B, Schad LR, Laun FB. Toward an optimal distribution of b values for intravoxel incoherent motion imaging. Magn Reson Imaging. 2011; 29(6):766–776. [PubMed: 21549538]
32. Boxerman JL, Schmainda KM, Weisskoff RM. Relative cerebral blood volume maps corrected for contrast agent extravasation significantly correlate with glioma tumor grade, whereas uncorrected maps do not. AJNR Am J Neuroradiol. 2006; 27(4):859–867. [PubMed: 16611779]
33. Donahue KM, Krouwer HG, Rand SD, et al. Utility of simultaneously acquired gradient-echo and spin-echo cerebral blood volume and morphology maps in brain tumor patients. Magn Reson Med. 2000; 43(6):845–853. [PubMed: 10861879]
34. Schmainda KM, Rand SD, Joseph AM, et al. Characterization of a first-pass gradient-echo spin-echo method to predict brain tumor grade and angiogenesis. AJNR Am J Neuroradiol. 2004; 25(9): 1524–1532. [PubMed: 15502131]
35. Cox RW. AFNI: software for analysis and visualization of functional magnetic resonance neuroimages. Comput Biomed Res. 1996; 29(3):162–173. [PubMed: 8812068]
36. Jenkinson M, Bannister P, Brady M, Smith S. Improved optimization for the robust and accurate linear registration and motion correction of brain images. Neuroimage. 2002; 17:825–841. [PubMed: 12377157]
37. Paulson ES, Schmainda KM. Comparison of dynamic susceptibility-weighted contrast-enhanced MR methods: recommendations for measuring relative cerebral blood volume in brain tumors. Radiology. 2008; 249(2):601–613. [PubMed: 18780827]

38. Bedekar D, Jensen T, Schmainda KM. Standardization of relative cerebral blood volume (rCBV) image maps for ease of both inter- and intrapatient comparisons. Magn Reson Med. 2010; 64(3): 907–913. [PubMed: 20806381]

39. Nyul LG, Udupa JK. On standardizing the MR image intensity scale. Magn Reson Med. 1999; 42(6):1072–1081. [PubMed: 10571928]

40. Padhani AR, Liu G, Koh DM, et al. Diffusion-weighted magnetic resonance imaging as a cancer biomarker: consensus and recommendations. Neoplasia. 2009; 11(2):102–125. [PubMed: 19186405]

41. Le Bihan D. Intravoxel incoherent motion perfusion MR imaging: a wake-up call. Radiology. 2008; 249(3):748–752. [PubMed: 19011179]

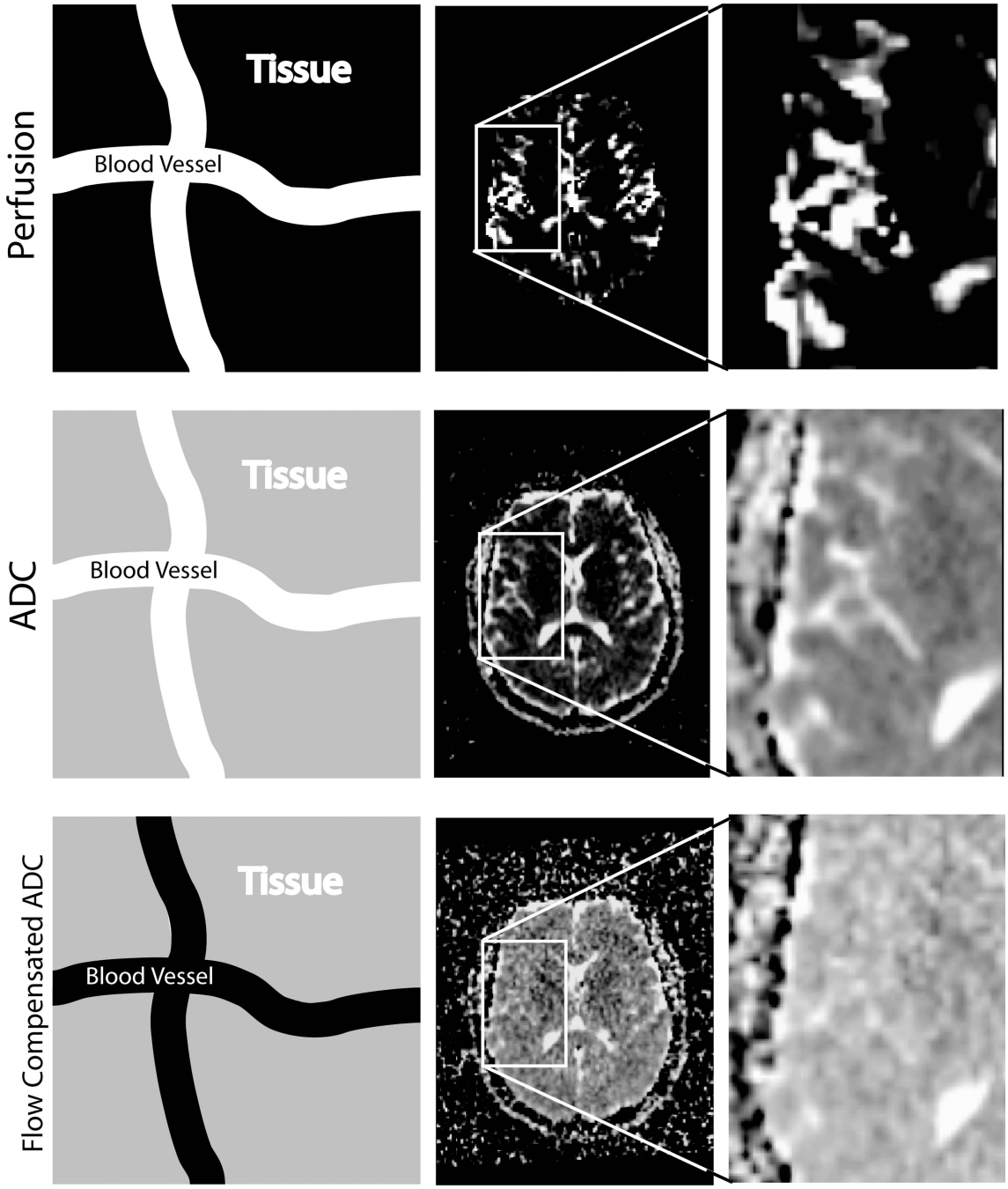

Figure 1.

The use of high b-values in the calculation of ADC reduces perfusion effects. In each row, the first image schematically represents the signal contributions within a voxel. A white color indicates a large contribution to the total signal, black indicates no contribution, and gray an intermediate contribution. The top row shows rCBV maps from one subject. Areas with high blood volume appear white. The middle row shows ADC calculated from b = 0 and 1000 s/mm^2. The blood vessels clearly contribute to the ADC value and are seen as high intensity in the ADC map. The bottom row shows flow compensated ADC calculated from b = 500 and 1000 s/mm^2. Here, signal from the blood vessels has been suppressed and they are no longer visible on the ADC map.

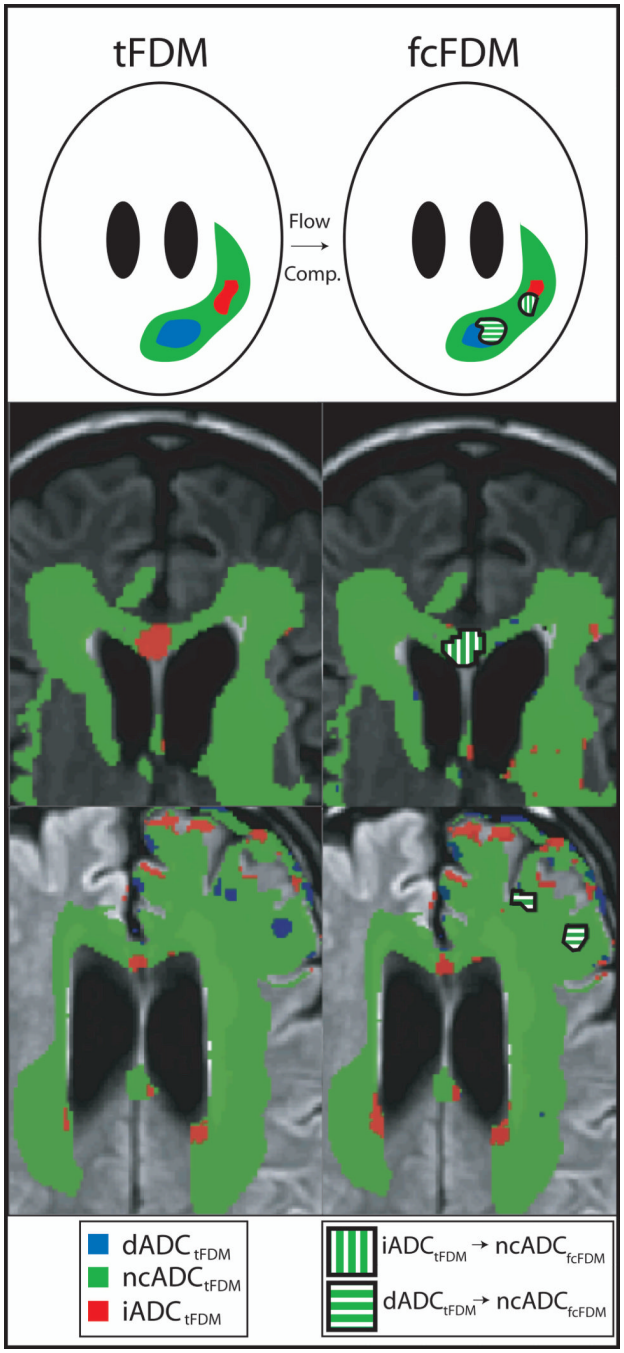

Figure 2.
Schematic and examples illustrating the differences between tFDMs and fcFDMs. Voxels classified as iADC, ncADC, or dADC are colored red, green, or blue respectively on the tFDM. Flow compensation eliminates the voxels on the tFDM that were shown to be iADC or dADC due to perfusion changes. These areas are shown as green with white stripes.

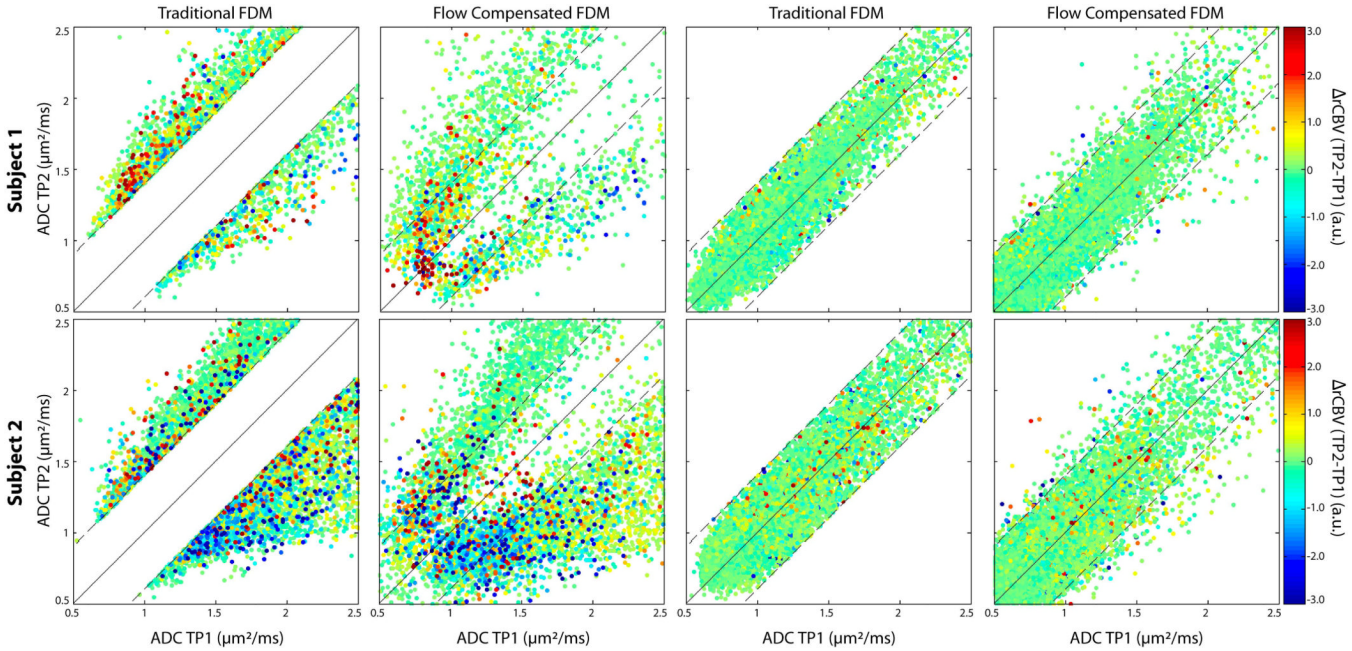

Figure 3.

FDM scatter plots. Each row shows FDM scatter plots from three representative patients, with each point representing one voxel. The horizontal axis is the ADC from TP1, the vertical axis is the ADC from TP2. The color of each point represents ΔrCBV from TP1 to TP2. Red and blue colors indicate an increase and decrease in rCBV respectively. Column 1 shows iADC and dADC voxels on the tFDM, and column 2 shows the *same* voxels on the fcFDM. Columns 3 and 4 show scatter plots of ncADC voxels on the tFDM and those *same* voxels on the fcFDM respectively

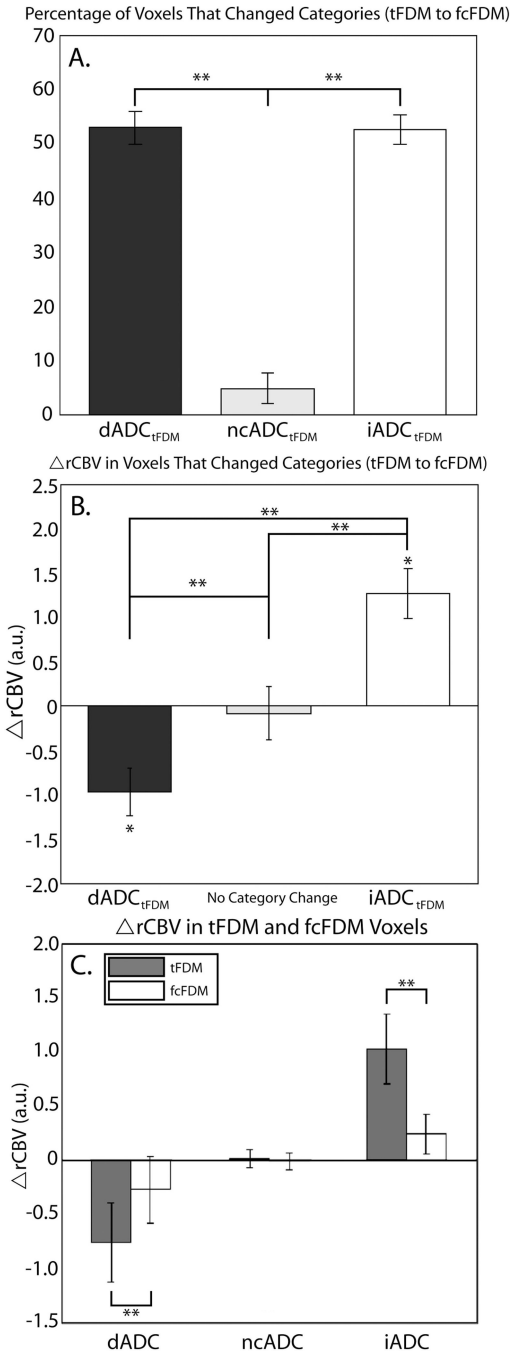

Figure 4.

A. The percentage of $iADC_{tFDM}$, $dADC_{tFDM}$, and $ncADC_{tFDM}$ voxels that changed categories from the tFDM to the fcFDM. **B.** Mean ΔrCBV in voxels that changed from $dADC_{tFDM}$ and $iADC_{tFDM}$ to $ncADC_{fcFDM}$ and mean ΔrCBV in voxels that did not change from the tFDM to the fcFDM. **C.** Mean ΔrCBV in $iADC_{tFDM}$, $dADC_{tFDM}$, and $ncADC_{tFDM}$ voxels compared to $iADC_{fcFDM}$, $dADC_{fcFDM}$, and $ncADC_{fcFDM}$ voxels respectively. * = significant difference via one-sample t-test, $p < 0.05$; ** = significant difference via two-sample t-test, $p < 0.05$.

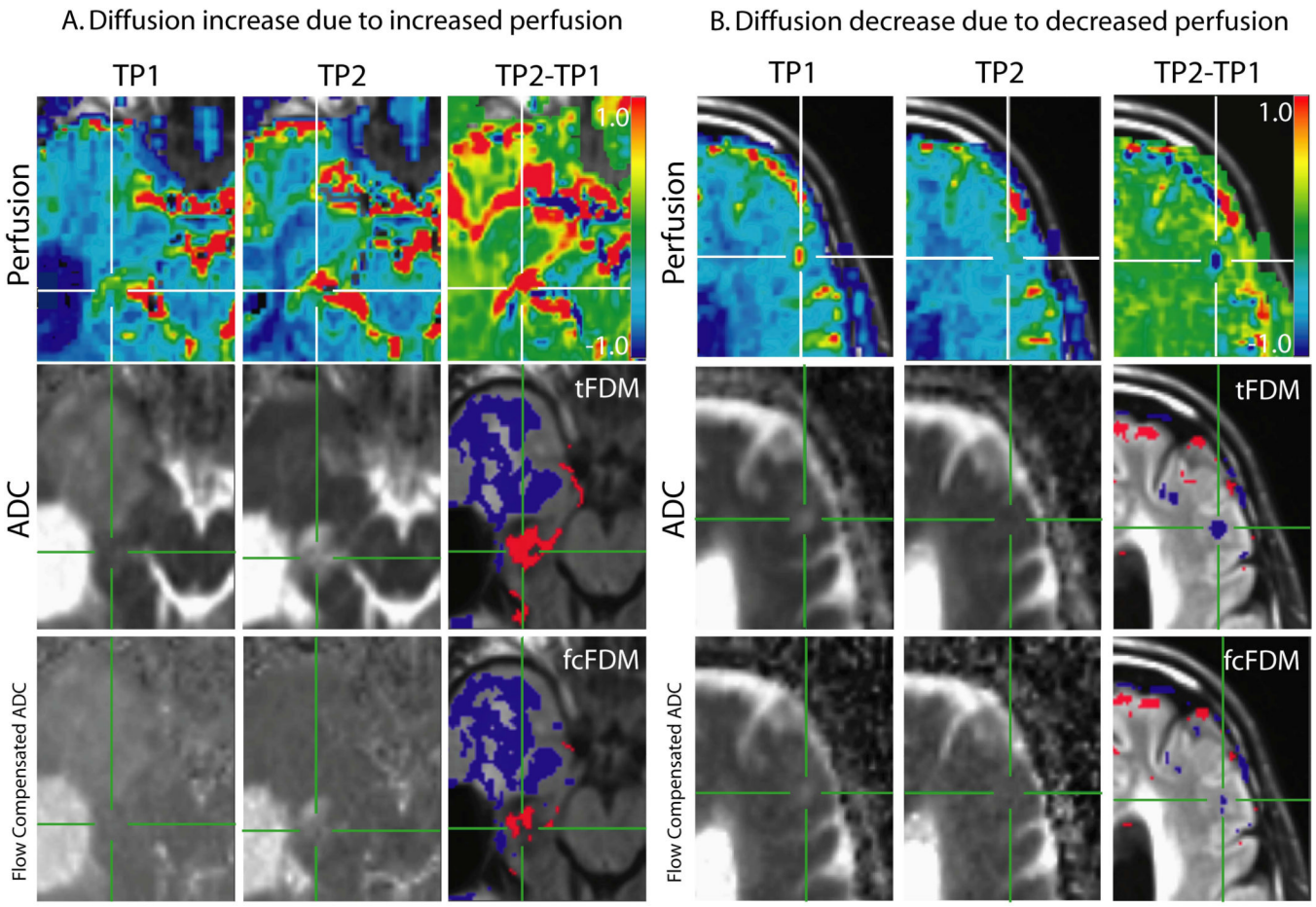

Figure 5.

Perfusion and diffusion maps in areas of significant changes in diffusion. The top row shows rCBV maps from TP1 and TP2 and the difference between the two (TP2-TP1, ΔrCBV). The middle row shows ADC calculated from b = 0 and 1000 s/mm^2 from TP1 and TP2 and the resulting tFDM. The bottom row shows the flow compensated ADC maps calculated from b = 500 and 1000 s/mm^2 from TP1 and TP2 and the resulting fcFDM. A. $iADC_{tFDM}$ voxels (red voxels) are due to an increase in perfusion rather than an increase in cellularity. In voxels that show up as $iADC_{tFDM}$ and $ncADC_{fcFDM}$ there is a corresponding increase in perfusion on the ΔrCBV map. B. $dADC_{tFDM}$ voxels (blue voxels) are due to a decrease in perfusion rather than a decrease an increase in cellularity. Where voxels show up as $dADC_{tFDM}$ and $ncADC_{fcFDM}$ there is a corresponding decrease in perfusion on the ΔrCBV map.

Table 1

Mean ΔrCBV values on tFDMs and fcFDMs

	iADC	dADC	ncADC	
ΔrCBV (tFDM)	1.02 (0.32)	−0.77 (0.36)	0.009 (0.080)	iADC>dADC ***; iADC>ncADC *; dADC<ncADC *
ΔrCBV (fcFDM)	0.24 (0.18)	−0.28 (0.31)	−0.02 (0.080)	N.S.
	***	**	N.S.	
% Classification Changing Voxels (tFDM → fcFDM)	52.6 (2.7)	52.9 (3.0)	4.7 (2.8)	iADC>ncADC ***;dADC>ncADC ***
ΔrCBV in Classification Changing voxels (tFDM → fcFDM)	1.26 (0.37) p = 0.0023	−0.97 (0.35) p = 0.010	−0.086 (0.25) p = 0.727	iADC>dADC **; iADC>ncADC *; dADC<ncADC *

Values are given in means (standard errors);

* p<0.05,

** p<0.01,

*** p<0.001;

N.S. = Not Significant; tFDM = traditional tFDM = traditional functional diffusion map; fcFDM = flow compensated functional diffusion map.